

# **DYNAMIC X-RAY MICRO-TOMOGRAPHY FOR REAL TIME IMAGING OF DRAINAGE AND IMBIBITION PROCESSES AT THE PORE SCALE**

Glenn R. Myers, Andrew M. Kingston, Trond K. Varslot, Michael L. Turner,  
Adrian P. Sheppard

Department of Applied Mathematics, Australian National University, Canberra, Australia

*This paper was prepared for presentation at the International Symposium of the Society of Core Analysts held in Austin, Texas, USA 18-21 September, 2011*

## **ABSTRACT**

The pore-scale imaging of fluid distributions during two-phase fluid displacements, such as drainage and imbibition, is of inestimable value for the validation of both experiment and modelling. Previous studies by several groups have shown that fluid distributions can be directly imaged at the pore scale with X-ray micro-CT. However, this work suffers the fundamental constraint that the sample must remain unchanging while each complete set of projections is acquired, a period from several minutes to several hours, depending on the instrument and the desired image quality. Any movement of the fluid-fluid interface that occurs during the data acquisition results in inconsistent projection data and degraded images.

To achieve a static system during a fluid displacement, one must halt the flood then wait for any transient movement to dissipate before acquiring image data and finally re-starting the experiment. This procedure significantly devalues the experiment since (a) one does not know how much interface relaxation has occurred during the waiting period, (b) one cannot study the effect of displacement rate with any confidence and (c) dynamic capillary effects such as contact angle hysteresis are likely to be lost.

In [7], we described a set of new “dynamic tomography” algorithms for the high-resolution, time-resolved imaging of continuous, complex processes such as two-phase fluid flow at existing X-ray micro-CT facilities. By exploiting geometric constraints inherent to the underlying physics, we are able to improve on current frame rates by at least an order of magnitude. Furthermore, we are able to image continually evolving systems without introducing artefacts.

To demonstrate this approach, we have conducted simple two-phase displacement experiments in Bentheimer sandstone. We present reconstructed 3D movies showing the evolution of the fluid distribution during these experiments, and discuss the drainage-imbibition hysteresis that is observed.

## INTRODUCTION

Historically, computed tomography (CT) has been used solely to image static samples [5]. An exception is medical imaging, where patient movement is often unavoidable, particularly when imaging organs like the heart or the lungs. One therefore needs to correct for these movements, forming a high-quality static image by removing the dynamic component [2]. In contrast, in the materials and geologic sciences the dynamic evolution itself is of genuine interest. For example, capturing the dynamics of multiphase fluid displacements in 3D would be of great value both because of the complexity of the underlying physics and because macro-scale experiments reveal little about the micro-scale processes. Experimental data is extremely expensive to obtain and returns frustratingly little information; modeling studies are cheaper and provide more insight but lack much predictive power. Finding out what happens at the micro-scale and comparing it with the predictions of modeling is sorely needed if the modeling is to become truly useful. Working within traditional limitations, existing efforts to image the pore-scale distribution of fluids during two-phase flow in porous materials have tried to ensure that the sample remained unchanging during the entire CT image acquisition, whether using synchrotron radiation [10,12,14] or lab sources [6,15].

X-ray CT is performed by collecting radiographs of a sample from a range of different viewing angles. From this data, a 3D image of the sample can be reconstructed, showing the 3D spatial distribution of X-ray linear attenuation coefficient [5]. Common (“classical”) methods for performing this inversion include filtered backprojection (FBP), Fourier inversion, and various iterative schemes such as algebraic reconstruction technique (ART), simultaneous iterative reconstruction technique (SIRT) and the related simultaneous algebraic reconstruction technique (SART) [9]. These classical algorithms all assume that the sample is static. If the sample changes during acquisition, the radiographs will be inconsistent with one another, leading to artefacts and/or blurring of the reconstructed image. In practice this means that classical CT imaging is restricted to situations where the sample is effectively static for the time it takes to acquire a full set of radiographs.

The inverse problem of classical CT reconstruction is well studied; it has been proven that radiographs at  $\approx \pi N/2$  viewing angles are required in order to accurately generate a 3D reconstruction on an  $N^3$  grid [8]. As the acquisition time for each radiograph is proportional to  $N^2$ , the maximum achievable time-resolution using classical CT reconstruction techniques is proportional to  $N^3$ , and is typically on the order of hours for a  $2048^3$  dataset using a lab-based micro-CT source. This is a fundamental limitation of classical CT: as the spatial resolution increases, so too does the amount of time the sample must remain essentially static. Synchrotron X-ray sources are capable of delivering massive X-ray doses in a short time. Unfortunately, the sample must still remain static whilst each scan is taken, and may be damaged/destroyed by the radiation dose well before the experiment is complete. Furthermore, synchrotron beamtime is a valuable commodity, providing a strong incentive to make more efficient use of the X-ray flux.

In discrete tomography (DT) it is assumed *a priori* that a static sample may be represented using only a few (usually two) gray levels. DT algorithms allow one to reconstruct samples from far fewer radiographs than would otherwise be required, leading to corresponding reductions in scan time and X-ray dose [1,4]. In particular, it has been shown that with appropriate *a priori* information about a static sample, it is possible to break the proportional relationship between the required number of radiographs and the spatial resolution of the reconstruction. This suggests that a suitably sophisticated reconstruction algorithm, that makes appropriate use of *a priori* information, will be able to image dynamic, continually evolving, samples at a high spatial and temporal resolution. In this paper, we move away from the “toy model” experiments of [7], which were intended to provide proof-of-concept of the reconstruction algorithm. We demonstrate the computational and experimental feasibility of this approach, as well as its relevance to fluid-displacement studies in porous rocks.

## EXPERIMENT AND DATA ACQUISITION

A simple experimental arrangement was used to enable air drainage of a water saturated sample inside a micro-CT instrument. The experiment arrangement is illustrated in Figure 1. A cylindrical piece of Bentheimer sandstone (porosity ~22%, permeability ~2500mD) 5mm in diameter and 12mm long was mounted to a hollow steel post using heatshrink. In between the sample and post (i.e. below the sample) was a 0.5mm thick glass fiber filter with 2 $\mu$ m pores to act as a capillary barrier. Above the sample was a few centimeters of heatshrink tube that was open to the air. Below the sample the hollow post was connected to a Water Swivel rotary joint to allow complete freedom of rotation. The non-rotating part of the apparatus consists of: (i) an MKS Baratron capacitive pressure sensor; (ii) 1800mm of air-filled 4mm diameter PTFE hose to act as a 25ml air piston; (iii) to which was connected a syringe pump. A 5ml syringe was used in the experiment. The imaging was performed using the original instrument at the ANU micro-CT facility [11], in operation since 2001.

The combination of a 25ml air piston and 5ml syringe was chosen so that the pressure below the sample (the “outlet pressure”) could be varied from 1.0 down to around 0.85bar by closing or opening the syringe, yielding a capillary pressure of 0 to 150mbar (~2.5psi). Pressure (rather than saturation) was therefore the independent variable in this experiment, and varied linearly with syringe position as long as the capillary pressure was much less than atmospheric pressure. Since the syringe was of much greater volume than the entire pore volume of the sample (30 $\mu$ l), the air piston allowed us to exert a finer control over the pressure than would otherwise have been possible. A direct low-volume flood with incompressible fluid only would also demand more of the vacuum sealing – the large air volume in our configuration makes it relatively insensitive to slow leaks or small air bubbles.

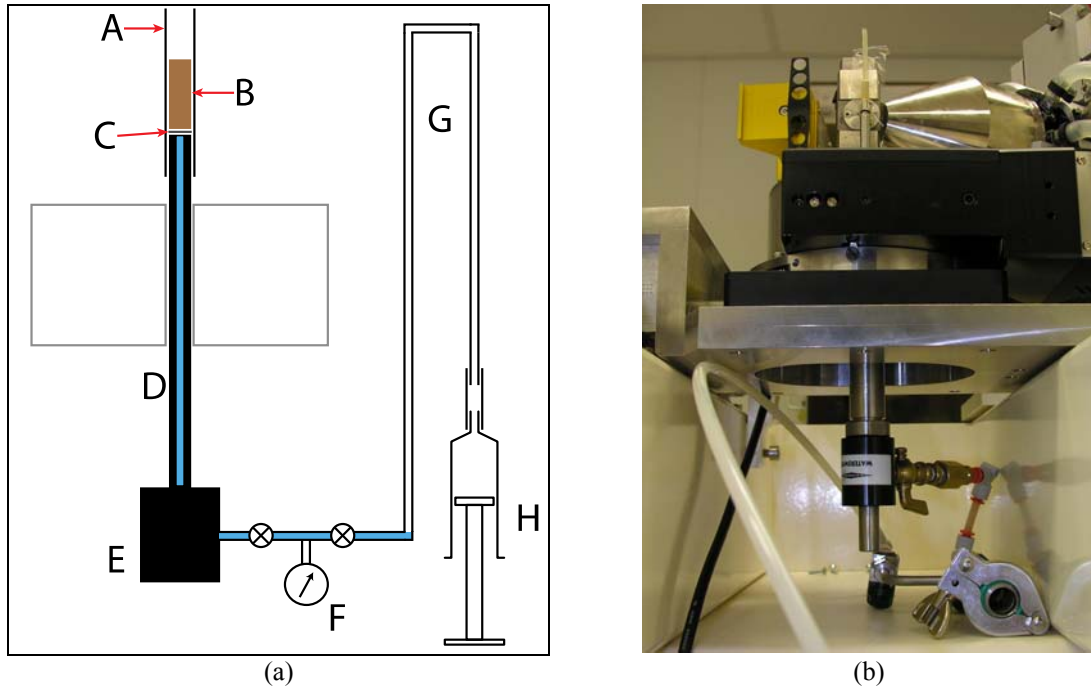


Figure 1 (a) Schematic of the experimental apparatus. A: heat-shrink around sample; B: 5mm cylindrical sample; C: capillary barrier; D: hollow sample post (passes through rotation stage); E: rotary joint; F: pressure sensor; G: 1800mm tubing gas piston; H: syringe pump. (b) Photo of apparatus installed in micro-CT, with sample near the top of the image and pressure sensor not installed. The white tubing in the foreground leads to the syringe pump that is out of the field of view.

The apparatus was assembled outside the instrument (minus air piston) and filled with a (degassed) aqueous solution of 0.25M potassium iodide as a contrast agent. To fully saturate the sample the tube near point G from Figure 1, where the gas piston would be attached, was connected to a reservoir of the water. At the same time a vacuum was applied at point A above the sample for about 1 hour, which drew about 5ml, or 120 pore volumes through the sample. The system was disconnected from the vacuum and fluid bath and installed in the  $\mu$ CT instrument (see Figure 1(b)), then the syringe pump was attached. A static image of the fully saturated configuration was taken at  $1024^3$ , using 1440 projections of 2.4s each for a tomographic acquisition time of 60 minutes. This image is shown in Figure 2(a). The drainage was then commenced by drawing back the syringe pump. We actuated the syringe pump controller at its slowest operating mode, resulted in full piston travel (i.e. scanning from  $P_c=0$  to 0.15mBar) being accomplished in around 2hrs. The peak of the Bentheimer throat radius distribution is approximately  $18\mu\text{m}$ , so that in an air-water drainage ( $\gamma=0.08\text{N/m}$ ,  $\theta=0^\circ$ ) most of the saturation change occurs between 60 and 80mBar. This pressure change occurs over about 15 minutes with our current configuration, which means that we need very good time resolution to capture the dynamics.

At the completion of the drainage run, when the syringe pump was at the end of its travel, another static image was acquired (Figure 2(b)). The pump direction was then reversed,

allowing the capillary pressure to drop and water to imbibe back into the sample. When the pump had returned to its original position the capillary pressure was slightly less than zero (i.e. the fluid below the sample was slightly overpressured) implying that the system had a small leak. The final fluid saturation after imbibition was  $S_w=0.75$ .

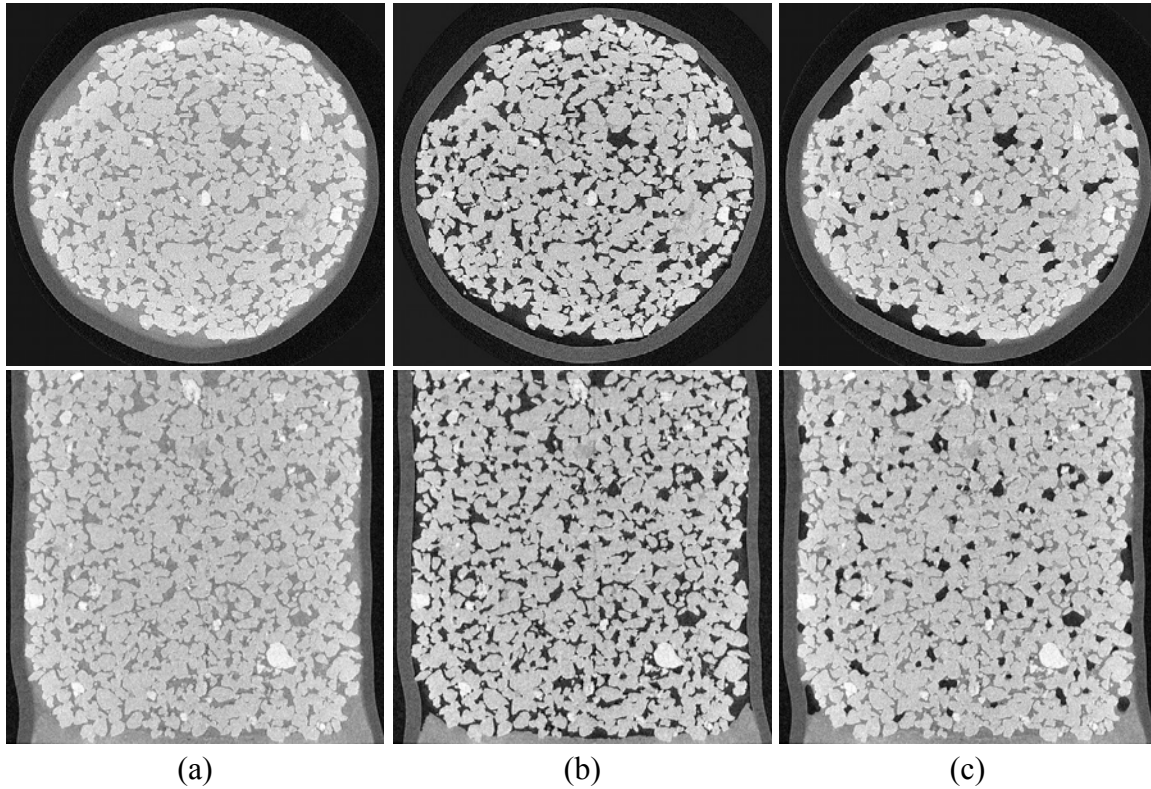


Figure 2: Slice images through static reconstructions of the initial and final conditions. (a) initial state,  $S_w=1.0$ ,  $P_c=0$ ; (b) after primary drainage  $S_w\approx 0$ ,  $P_c=180\text{mBar}$ ; (c) after imbibition,  $S_w=0.75$ ,  $P_c=0$ . The sample diameter is 5mm; scans were performed at  $1024^3$  with  $6\mu\text{m}$  voxel size, but downsampled to  $512^3$  with  $12\mu\text{m}$  voxel size before use. The glass fiber capillary barrier is visible at the bottom of the sample.

## DYNAMIC CT RECONSTRUCTION METHOD

Our approach is to factor out the static features of the sample and concentrate on the relatively small changes occurring between one moment and the next. Intuitively, this is similar to motion picture encoding, where the dynamic signal is encoded using as little data as possible. The usage of data compression schemes in reconstruction problems (referred to as “compressed sensing”, or CS) has a sound mathematical foundation [3]. A sub-class of CS methods treat reconstruction as an optimisation problem where one aims to minimize a cost function that is an appropriately weighted combination of: (i) the discrepancy between the solution and the measured data; and (ii) the “total variation” (i.e., the  $L^1$  norm of the gradient) of the solution. Similarly, we formulate the dynamic tomography algorithm as an optimisation problem, given appropriate constraints, which results in a method for “dynamic” (i.e., 4D) CT imaging of time-evolving samples. This method is particularly well adapted for the imaging of immiscible displacements of

incompressible fluids for which the *a priori* information is highly constraining, as we shall see.

We conceptually separate our sample into: (i) the static Bentheimer sandstone, which is structurally complex; and (ii) the dynamic fluid distribution, about which we possess appropriate *a priori* information. This *a priori* information is as follows: (i) the fluids are relatively incompressible, and so each fluid will exist only at a single grey level; and (ii) the sandstone is impermeable to fluid, so fluid can be found only within the pore-space of the rock. Condition (i) is strictly true for the water phase, and effectively true for the gas since its attenuation is indistinguishable from a vacuum at all times. Condition (ii) would be violated in any regions of microporosity. While there are in fact some “microporous” regions in Bentheimer when imaged at a 10 $\mu$ m voxel size, we expected and found that these regions remained water saturated at all times at the moderate capillary pressures used here. As in Discrete Tomography and Compressed Sensing, this *a priori* information is used to help reconstruct the dynamic fluid distribution from incomplete measurements, effectively taking the place of the missing data.

As detailed in [7], we use an iterative SIRT-based reconstruction algorithm which attempts to optimize, over the space of all two-gray-level solutions consistent with the static pore structure, the following quality measures: (i) the discrepancy between the solution and the measured data; and (ii) the spatial localization of the solution. The majority of the algorithm was implemented in Python 2.6 and particularly Scientific Python, with the exception of the projection and backprojection operations that form part of SIRT. Projection and backprojection are (at least) an order of magnitude more computationally complex than any other step in the algorithm, and so were implemented in CUDA 4.0. While this is, in principle, a prototype configuration, the most computationally intensive parts are performed in libraries that are written in C/C++ or CUDA, so the performance disadvantage of using an interpreted language is small.

This algorithm was run on 8 of the GPU-enabled nodes of the xe supercomputer at the ANU National Computing Infrastructure National Facility (NCI-NF). In total, we made use of 4 quad-core 3.0GHz Intel Harpertown CPUs, 16 nVidia Tesla s2050 GPUs, and 90GB of RAM.

## RESULTS AND DISCUSSION

As described above, the experimental sequence consisted of (i) initial static image, (ii) dynamic imaging of air drainage, (iii) static image of the drainage endpoint, (iv) dynamic imaging of water imbibition and (v) a static image of the trapped gas after imbibition. The three static images each needed 60 minutes to acquire, while during the 2 hours of each fluid displacement, the stage rotated about 100 times, with 72 projections of 0.8s exposure time being acquired during each revolution, at 5° spacing. To minimise motion blurring the rotation stage did not rotate continuously, but was allowed 0.4s to move between projection angles. The full experiment time was about 12 hours. Dynamic (4D) reconstructions were made of both the drainage and the imbibition data, using support data from the relatively dry drainage-endpoint image shown in figure 2(b), and

differencing the dynamic projections against the starting point static projections for both experiments. The dynamic reconstruction algorithm ran for approximately 1 hour 45 minutes of which 54 minutes were devoted to projection and backprojection steps. Over the course of each 4D reconstruction, approximately 300,000  $512^2$  pixel projections were generated from  $512^3$  voxel volumes, with an equivalent number of backprojections. This is far quicker than it would have taken using an optimized CPU-based algorithm written in C.

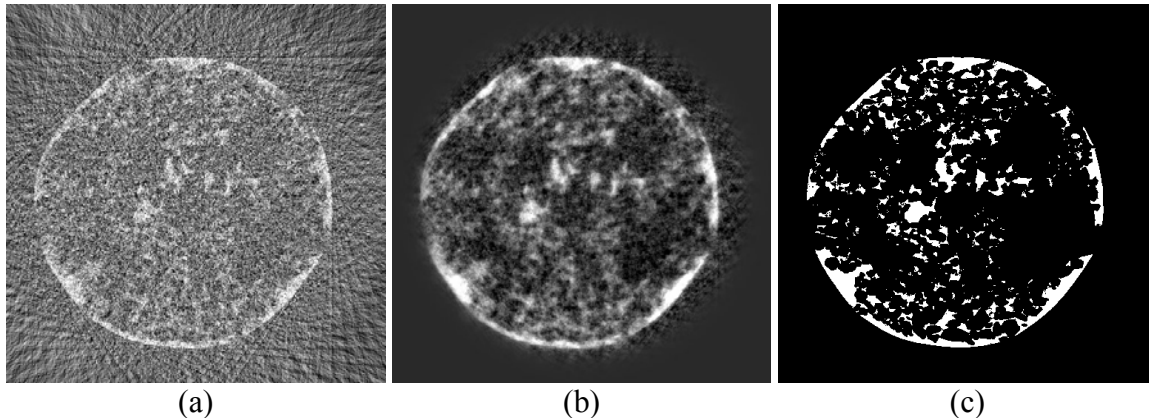


Figure 3: Slice through a reconstructed volume obtained using (a) standard FDK filtered backprojection, (b) standard SIRT iterative reconstruction, (c) the new algorithm described here, including support constraints, spatial sparsification and binarisation. These images are reconstructed from 72 projections at  $5^\circ$  increments taken in 85 seconds, rather than 720 projections at  $0.5^\circ$  increments taken over 25 minutes that would be normal for a  $512^3$  scan.

Figure 3 presents a single slice from near the halfway point in the drainage run, reconstructed using three different methods. It can be seen that our new method, which integrates segmentation and reconstruction, is a significant advance over existing methods. Slices through several frames from the reconstructed drainage dataset are shown in Figure 4. Animations of slices from all frames in animated gif form along with rendered 3D rendered movies of the invasion (generated with Drishti visualisation software) can be found at <http://xct.anu.edu.au/MyersSCA2011>. Figure 5 shows capillary pressure curves for the drainage and imbibition runs. The drainage curve is largely as expected, with the majority of the saturation change occurring at around 50mbar. This is slightly less than we would expect, particularly given that the dissolved salt has slightly increased the air-water surface tension. Also, the drainage endpoint is at essentially zero water saturation, a consequence of the  $12\mu\text{m}$  resolution that was unable to capture water layers/menisci. The imbibition  $P_c$  curve, on the other hand, is quite unphysical as the saturation change occurs at a significantly *higher*  $P_c$  than the drainage, and over a smaller range of pressures. This indicates a fault in the experiment rather than the reconstruction, since it represents an error in the pressure measurement and control, rather than an error in the saturation. Finally, Figure 6 presents images of some imbibition data, while Figure 7 compares fluid distributions from drainage and imbibition at the same water saturation. The imbibition data is less convincing than the drainage data; more analysis and further experiments are required.

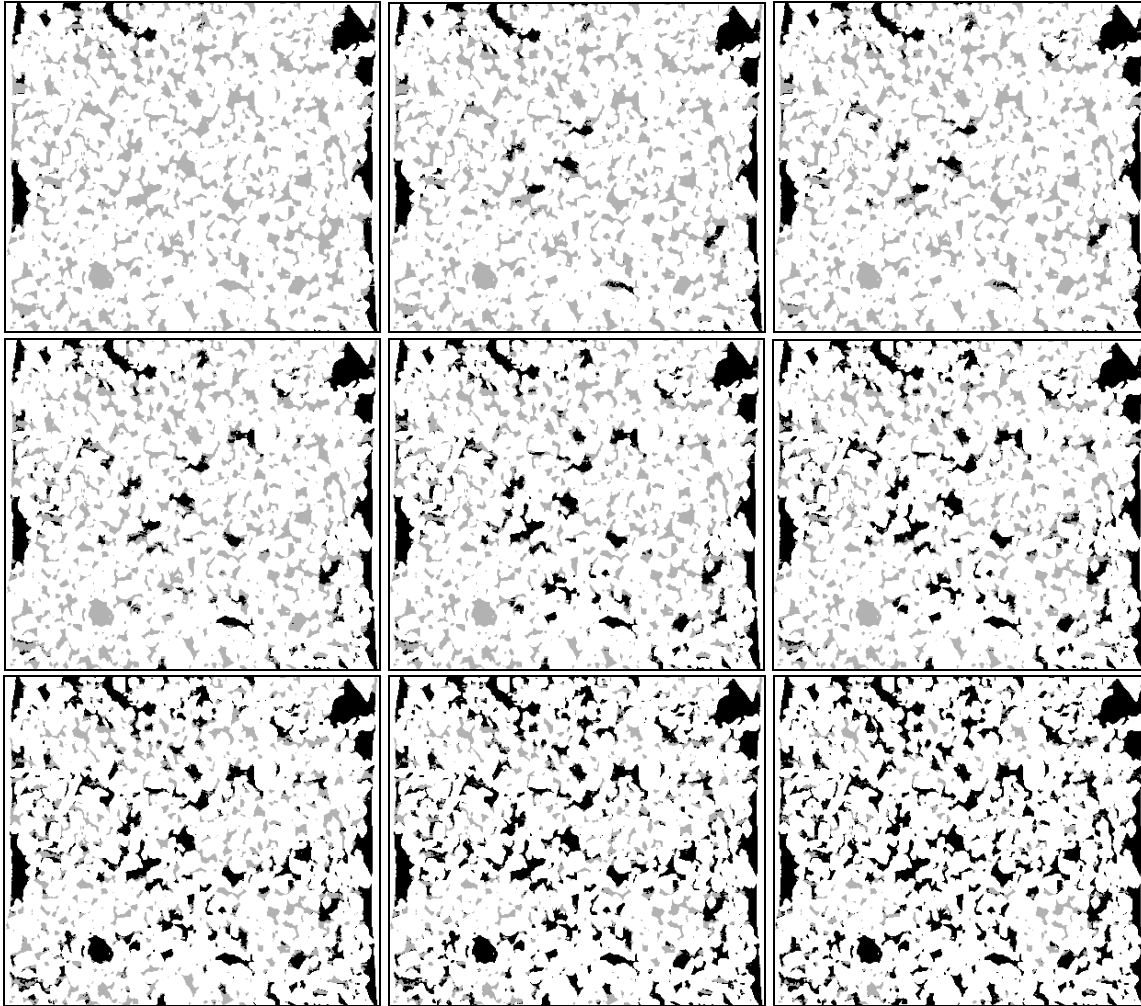


Figure 4: Slice through the dynamic reconstructed data at 9 successive frames (frames 18 to 26 out of 38) during the drainage. Air is black, water is grey, grains are white. The ability of the method to capture Haines jump type displacements is seen by the complete drainage of the large pore in the lower left in a single time step. Note that the grain phase is derived from the static image shown in figure 2(b).

The imaging quality could be improved by increasing the concentration of contrast agent. This had been chosen to give enough contrast in normal imaging without causing unnecessary beam hardening. Experience had shown that higher concentrations of contrast agent affected the polychromatic beam of our X-ray source to adversely affect image subtraction. However, since beam hardening effects will be less severe when differencing adjacent images with only a small difference in saturation, we will use a higher salt concentration in future. This may have consequences for the interfacial properties of the system – certainly it precludes the investigation of lo-sal waterflooding, for example. Another option is to use an organic contrast agent such as iodododecane which allows the use of water of any salt concentration.

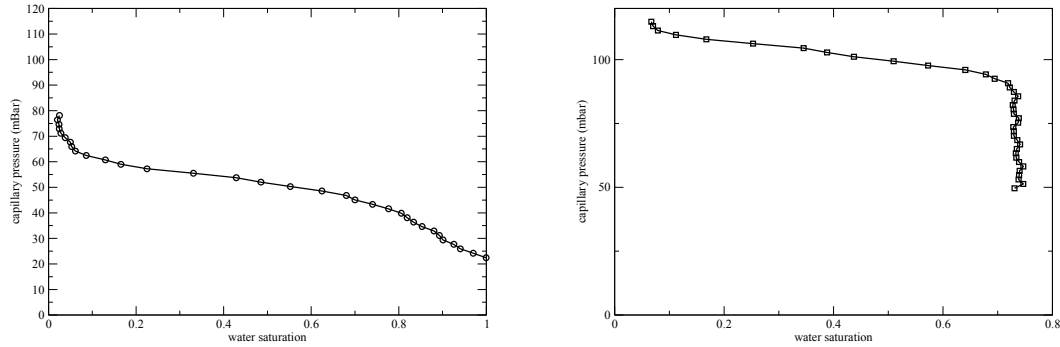


Figure 5: Capillary pressure curves. where the pressure data is measured experimentally but the fluid saturation is taken from the reconstructed images. (a) drainage, (b) imbibition. The drainage continued to a capillary pressure of 240mBar with no further measurable change in saturation; the imbibition run then commenced. The very low water saturation at the drainage endpoint is a consequence of being unable to resolve wetting menisci at this resolution. The higher pressure in the imbibition curve is unphysical and indicates an unresolved experimental problem.

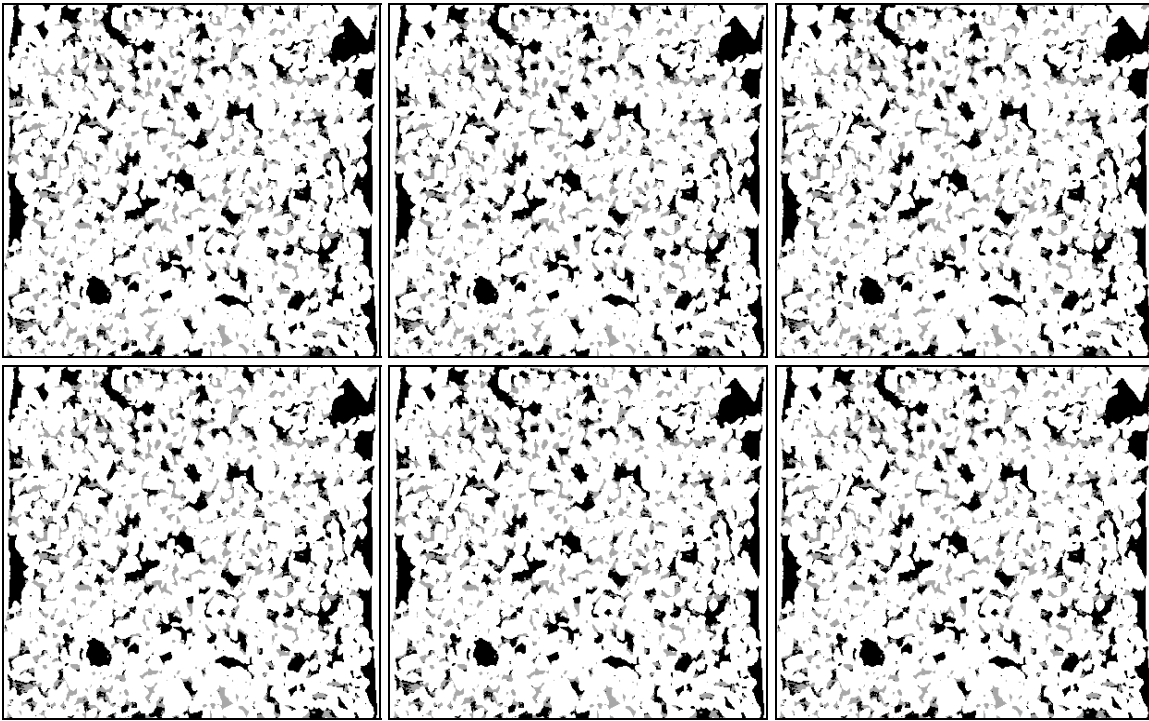


Figure 6: Some slice images from the dynamic reconstruction of the imbibition run.

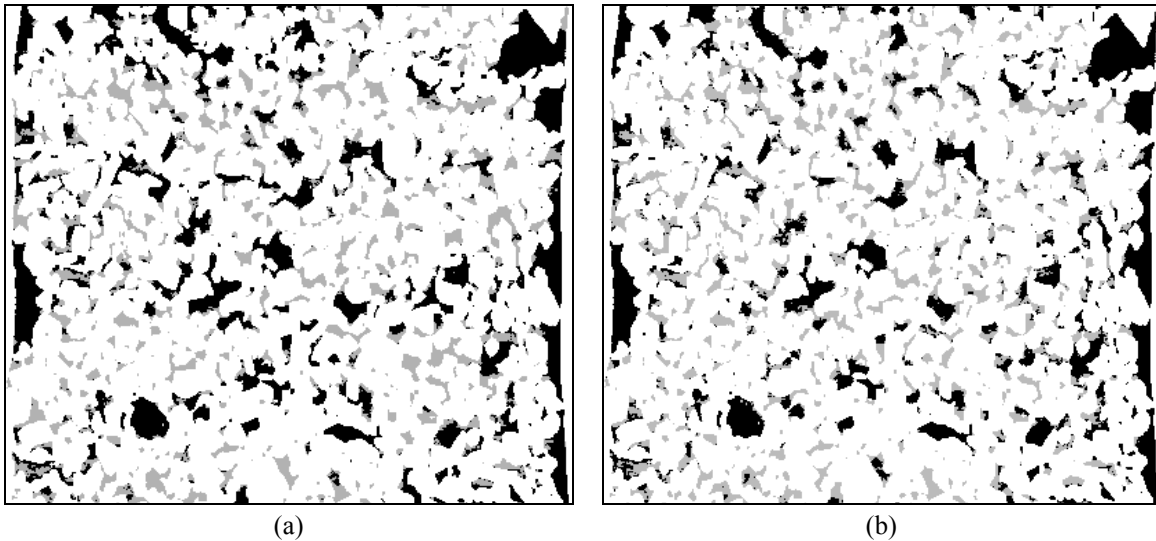


Figure 7: a comparison of (a) drainage and (b) imbibition where  $S_w=0.6$ . Significant differences (i.e. hysteresis) can be observed, particularly more partially filled pores for imbibition.

Unfortunately, it is not yet possible to calculate properties like resistivity index (RI) or unsteady state relative permeability from this data. This is primarily because the image resolution is simply inadequate - at  $512^3$  the voxel size is  $12\mu\text{m}$ , which cannot capture enough detail when the principal channel radius is less than  $20\mu\text{m}$ . In addition, largely due to the low fluid contrast, the segmented data from the dynamic reconstructions is still reasonably noisy, which at this voxel size has a dramatic effect on the transport properties. The calculation of a wetting phase property like RI would require data of significantly higher resolution and lower noise. We are confident that this can be obtained by increasing fluid contrast and combining dynamic reconstruction with high cone-angle helical scanning [13]. We therefore consider the computational resources that would be required in the reconstruction of dynamic data sets at a higher resolution of  $1024^3$ . RAM usage will scale with  $N^3$ , so that will increase by a factor of eight, meaning that processing must either be done on a cluster ( $\sim 800\text{GB}$  of RAM), or with significant parts of the data being cached to disk at each iteration. Note that our implementation was not optimised for RAM usage, so this should be considered an upper limit. Processing time, on the other hand, will scale with  $N^4$ , thus increasing by a factor of sixteen, to about 14 hours if 32 GPUs were used; still an acceptable processing time given the duration of the experiments. A compute cluster providing this capability could be purchased for under US\$100,000, far less than the cost of the imaging hardware.

The experiments presented here suffer from the fact that we were unable to acquire reference images at each time step whose accuracy was assured and therefore we cannot be certain of the fidelity of the dynamic imaging. Therefore our immediate plan is to repeat these experiments at a much slower flow rate so that extensive redundant data can be acquired, allowing the reconstruction of high quality reference images. This experiment will enable us to quantify the accuracy of the dynamic reconstructions.

## CONCLUSION

We have demonstrated the use of a new technique for tomographic imaging of drainage and imbibition processes that reduces the acquisition time compared with traditional techniques by an order of magnitude and allows artefact-free imaging of time-changing data. In particular, we show that sophisticated iterative reconstruction techniques are computationally feasible on images up to  $1000^3$ , in the sense that the cost of enabling a micro-CT facility with the necessary computer hardware will be a small outlay relative to the cost of the facility. After applying the technique with reasonable success to gravity-dominated drainage of 2mm spheres in a previous work, we have performed preliminary experiments of air-water drainage and imbibition on a 5mm Bentheimer sandstone, obtaining  $512^3$  images at 80-second time intervals. The results showed that one can track the invasion front with enough precision to determine which pores are filled at any moment in time.

This is preliminary work, and there is much to do before this method can be used in production. In the near-term future we plan to run the experiment sufficiently slowly to evaluate the accuracy of the dynamic reconstruction, and to improve image quality by using higher contrast fluids and integrating with high-cone-angle helical scanning.

## ACKNOWLEDGEMENTS

We acknowledge the financial support of the member companies of the ANU/UNSW Digital Core Consortium, and to the Australian Research Council who provided funding through grants DP110102964 and FT100100470. Compute resources were provided through an ANU partner share grant allocation on the National Facility of Australia's National Computing Infrastructure. Thanks also to Andrew Fogden and Jill Middleton for valuable discussions, to Benjamin Young for assistance with sample preparation and imaging and to Ajay Limaye for Drishti animations.

## REFERENCES

1. Batenburg, K., "A network flow algorithm for binary image reconstruction from few projections," *Lecture Notes in Comput. Sci.*, (2006) **4245**, pp. 86-97.
2. Bonnet, S., Koenig, A., Roux, S., Hugonnard, P., Guillemard, R. and Grangeat, P., "Dynamic X-ray Computed Tomography," *Proceedings of the IEEE*, (2001) **91**, pp. 1574–1587.
3. Chen, G., Tang, J. and Leng, S., "Prior image constrained compressed sensing (PICCS): A method to accurately reconstruct dynamic CT images from highly undersampled projection data sets," *Med. Phys. Lett.*, (2008) **35**, pp. 660-663.
4. Herman, G. and Kuba, A., Eds., *Discrete Tomography: Foundations, Algorithms and Applications*. Birkhauser, Boston (1999).
5. Kak, A. and Slaney, M., *Principles of Computerized Tomographic Imaging*. SIAM, Philadelphia (2001).

6. Kumar, M., Senden, T., Knackstedt, M., Latham, S., Pinczewski, V., Sok, R., Sheppard, A., Turner, M., “Imaging of Pore Scale Distribution of Fluids and Wettability,” in *22nd International Symposium of the Society of Core Analysts*, Abu Dhabi, UAE, 2008.
7. Myers, G., Kingston, A., Varslot, T., Turner, M., and Sheppard, A., “Dynamic Tomography with a priori information,” *Applied Optics*, (2011) *in press*.
8. Natterer, F., *The Mathematics of Computerized Tomography*. Society for Industrial and Applied Mathematics, Philadelphia (2001).
9. Natterer, F. and Wübbeling, F., *Mathematical Methods in Image Reconstruction*. Society for Industrial and Applied Mathematics, Philadelphia (2001).
10. Prodanovic, M., Lindquist, W. and Seright, R., “3D image-based characterization of fluid displacement in a Berea core,” *Advances in Water Resources*, (2007) **30**, pp. 214-226.
11. Sakellariou, A., Senden, T., Sawkins, T., Knackstedt, M., Turner, M., Jones, A., Saadatfar, M., Roberts, R., Limaye, A., Arns, C., Sheppard, A., Sok, R., “An X-ray tomography facility for quantitative prediction of mechanical and transport properties in geological, biological and synthetic systems,” *Developments in X-ray Tomography IV*, (2004) **5535**, pp. 473–484.
12. Scheel, M., Seemann, R., Brinkmann, M., Di Michiel, M., Sheppard, A., Breidenbach, B., Herminghaus, S., “Morphological clues to wet granular pile stability,” *Nature Materials*, (2008) **7**, pp. 189-193.
13. Varslot, T. K., Kingston, A. M., Latham, S. J., Middleton, J., Knackstedt, M. A. and Sheppard, A. P. “Combining high-fidelity helical micro-tomography with region-of-interest scanning for improved core characterization,” presented at the *25th International Symposium of Core Analysts*, Austin, TX, USA, 18-21 September 2011.
14. Wildenschild, D., Hopmans, J., Rivers, M. and Kent, A., “Quantitative analysis of flow processes in a sand using synchrotron-based X-ray microtomography,” *Vadose Zone Journal*, (2005) **4**, pp. 112.
15. Youssef, S., Han, M., Bauer, D., Rosenberg, E., Bekri, S., Fleury, M., Vizika, O., “High Resolution  $\mu$ -CT combined to numerical models to assess electrical properties of bimodal carbonates.” in *22nd International Symposium of the Society of Core Analysts*, Abu Dhabi, UAE, 2008.